Electronic Supplementary Information for:

Phenomenological observations of quinone-mediated zinc oxidation in an alkaline environment

Christopher T. Mallia and Fikile R. Brushett

Experimental Details:

Experimental electrochemical work was collected using aqueous electrolytes comprised of semiconductor grade potassium hydroxide (KOH) (Sigma Aldrich, 99.99% excluding sodium), Millipore Sigma deionized water (18.2 MΩ) and 50 mM concentrations of either 2-hydroxy 1,4-naphthoquinone (Alfa-Aesar, 98%), 2,6-dihydroxyanthraquinone (AK Scientific, 98%), or 2,5-dihydroxybenzoquinone (Sigma-Aldrich, 98%). All chemicals were used as received (stored in a nitrogen (N_2) drybox), and allowed to dissolve to final concentrations for at least 24 h prior to experiments. Due to the potential light sensitivity of the redox mediators used, semi-opaque HDPE (high-density polyethylene, Wheaton) scintillation vials were used for storage to minimize ambient illumination, and to prevent glass corrosion. During and between measurements, all electrolytes were sparged with humidified nitrogen gas (dried gas passed through deionized Millipore water), with blanketing (sparging in headspace) done during measurements to prevent disruptions of diffusional mass transport. This was done for at least 10 minutes prior to collecting any data and prior to introduction of zinc surfaces to electrolyte.

Voltammetry was performed with a 2-mm diameter platinum (Pt) disk electrode (CH Instruments) or 10-µm diameter Pt microelectrode (BASi), a Hg/HgO reference electrode (1 M KOH, BASi), and a Pt wire counter (CH Instruments). Zinc (Zn) electrodes (2-mm diameter) were made from Zn metal wire (99.95%, unannealed, Alfa Aesar). Wires were cut, quickly mounted onto pre-soldered copper wire (99.9%, McMaster Carr), with sufficient room and minimal time to prevent extensive heating in the Zn wire, and then sealed into a PTFE shroud (McMaster Carr) with metallographic mounting epoxy (Pace technologies). The ends of these electrodes were then polished sequentially by SiC sandpaper (McMaster Carr) down to 0.05 µm alumina aqueous polishing slurry (Buehler). All electrodes were then thoroughly rinsed with ACS grade (>99.5%) acetone and isopropanol, sonicated in DI water for several minutes, dried with N_2, and stored under dry N_2 until use. A CH instruments 760E potentiostat was used for all electrochemical measurements, and all were performed at room temperature. Cyclic voltammetry was conducted at varying scan rates (10, 25, 50, 100 mV/s) for quinone species, with intermissions for stirring and sparging with humidified nitrogen gas between scan rates. Measurements were collected at each scan rate 3 times. For Zn electrode data, Mott-Schottky plots, OCP and potentiostatic impedance spectra (5 mV amplitude, -1.375 V vs Hg/HgO, 100 mHz to 100 kHz at 12 points per decade) were collected on the same Zn electrode vs a Hg/HgO reference and vs a Pt counter. Optical microscopy was conducted using a homemade cross-polarized setup on a metallurgical microscope (AMscope), using a camera calibrated with a micrometer scale, with images collected

in the Amscope software. Samples were either imaged immediately after experiments, or stored under dry N_2 until imaging was possible.

Schematic Figure of Redox-Mediated Reaction (Figure S1)

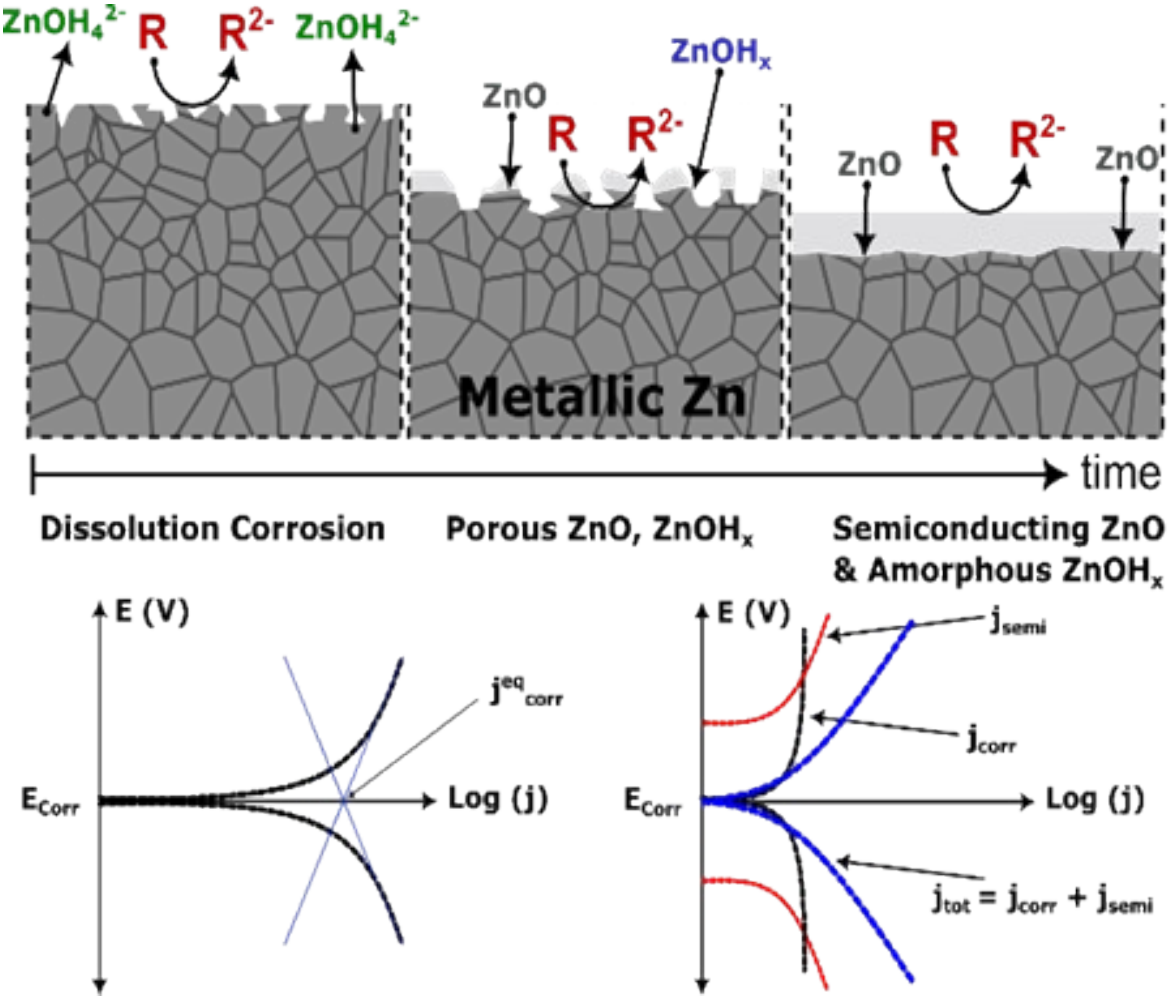

Figure S1. Schematically shows the evolution of the zinc metal surface, and the multiple processes that can progress in parallel. The initial stages are classic corrosion, evinced by pitting and crevice-corrosion, followed by film growth of an amorphous and crystalline oxide layer. At later stages, the surface is functionally covered, and charge transport through the solid film, in this case semiconducting ZnO, can occur. Two distinct polarization dependent charge transfer reactions can therefore occur, in parallel. In red, conduction band electron transfer. In black, classic Butler-Volmer or Tafel like-behavior for an outer-sphere electron transfer (corrosion). In blue, the rough linear superposition of the two mechanisms results in a larger net current than from one alone.

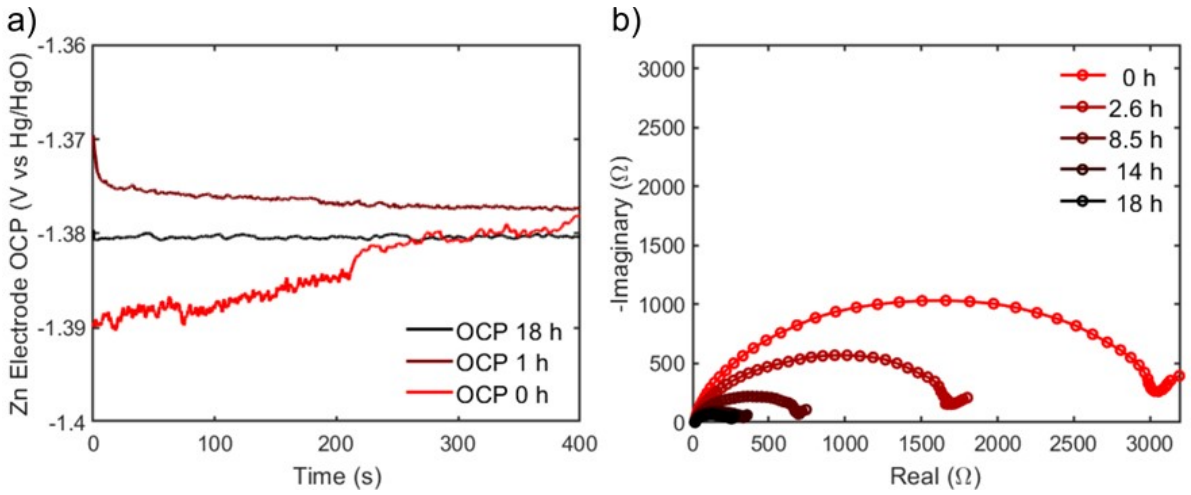

Figure S2. (a) Open circuit potential measurements performed on the zinc electrode at time points corresponding to the images presented in Figure 2 in the main text. (b) Select Nyquist plots from electrochemical impedance spectroscopy measurements taken at open circuit conditions and at similar time points in progression with the images of Figure 2 in the main text. Geometric area for Zn electrode was 0.126 cm^2, however increase in real surface area due to corrosion was difficult to quantify, but evident in decrease of charge transfer resistance.

Corrosion reaction associated with zinc metal (Scheme 1)

$$Zn(s) + 4OH^-(aq) \leftrightarrow Zn(OH)^{2-}_4(aq) + 2e^-$$
$$Zn(OH)^{2-}_4(aq) \leftrightarrow ZnO(s) + H_2O + 2OH^-(aq)$$

Full compound names and discussion of reactions for quinone derivatives:

All quinone compounds used in this study were purchased from commercial vendors and used as received (see experimental details). Tables S1 and S2 detail the reduction potentials and reaction involving each quinone as a two-electron reduction reaction, for which the half-wave potential is believed to be representative. All species possess pKa values significantly below 14[1–3] indicating that in 1 M KOH all hydroxyl groups are expected to be deprotonated. This deprotonation can consume up to 2 hydroxyl ions in the case of DHAQ and DHBQ, while consuming 1 hydroxyl in the case of HNQ. While this is anticipated to impact performance at elevated concentrations, the quinone concentrations described here were limited to 50 mM, indicating a decrease in the hydroxyl species concentration of at most 10%, or a pH value of 13.95. None of the species are commercially available in reduced form, owing to their instability in ambient air.

Table S1.

Hydroxynaphthoquinone			
Scan Rate (mV/s)	Peak Anodic (V vs Hg/HgO)	Peak Cathodic (V vs Hg/HgO)	$E_{1/2}$ (V vs Hg/HgO)
10	-0.593	-0.655	-0.624
25	-0.592	-0.657	-0.625
50	-0.591	-0.657	-0.624
100	-0.590	-0.657	-0.624
Average $E_{1/2}$ (vs Hg/HgO)			-0.624
Average $E_{1/2}$ (vs SHE)			-0.524
Dihydroxybenzoquinone			
Scan Rate (mV/s)	Peak Anodic (V vs Hg/HgO)	Peak Cathodic (V vs Hg/HgO)	$E_{1/2}$ (V vs Hg/HgO)
10	-0.814	-0.872	-0.843
25	-0.803	-0.877	-0.840
50	-0.797	-0.880	-0.839
100	-0.814	-0.886	-0.850
Average $E_{1/2}$ (vs Hg/HgO)			-0.843
Average $E_{1/2}$ (vs SHE)			-0.743
Dihydroxyanthraquinone			
Scan Rate (mV/s)	Peak Anodic (V vs Hg/HgO)	Peak Cathodic (V vs Hg/HgO)	$E_{1/2}$ (V vs Hg/HgO)
10	-0.788	-0.866	-0.827
25	-0.786	-0.870	-0.828
50	-0.785	-0.870	-0.828
100	-0.786	-0.872	-0.829
Average $E_{1/2}$ (vs Hg/HgO)			-0.828
Average $E_{1/2}$ (vs SHE)			-0.728

While deprotonation of hydroxyl groups results in a net negative charge for the quinone species in solution (and a resultant change in solvation structure), we elect for simplicity of discussion to only include the charges involved in electron transfer in our naming scheme. In short, we equate $DHAQ^{-4}/DHAQ^{-2}$ at pH 14 to $DHAQ^{-2}/DHAQ$ rather than explicitly state negatively charged species in the “oxidized” form.

Table S2.

Species	Full Name	Reduction reaction	Diffusion Coefficient (cm^2/s)	Measured $E_{1/2}$ (Half-wave potential, V vs SHE)
HNQ	2-hydroxy 1,4-naphthoquinone	$HNQ + 2e^- \leftrightarrow HNQ^{2-}$	*4.5-6.1 × 10^{-6} [1,4]	-0.524
DHAQ	2,6-dihydroxyanthraquinone	$DHAQ + 2e^- \leftrightarrow DHAQ^{2-}$	4.8 × 10^{-6} [2]	-0.727
DHBQ	2,5-dihydroxybenzoquinone	$DHBQ + 2e^- \leftrightarrow DHBQ^{2-}$	3.7 × 10^{-6} [3]	-0.742

* Values reported as a range between bislawsone dimer in 1 M KOH and HNQ in 1 M NaCl.

Discussion of corrosion products for Zn anodes

From the prior literature,[5–7] it is well-known that Zn anodes will corrode at high pH to form both soluble and insoluble components, which form a surface passivation layer (see for example reaction scheme 1). Extensive studies have indicated the possible formation of several amorphous zinc hydroxide solid phases, and crystalline ZnO, in addition to soluble zincate ionic species. These latter soluble species are anticipated to saturate in the electrolyte and form insoluble solid species as a product.[8,9]

This information was considered, along with XRD data reported by Fenton et al[10], to suggest possible surface species from the reaction with quinone. XRD data confirmed the presence of ZnO as a corrosion product, but would be insensitive to soluble ionic species. In the presence of quinone mediator, XRD also indicated the presence of $Zn(OH)_2$ species, but given the uncertainty in quantifying all present solid surface species, we elect to generalize hydroxide components as $Zn(OH)_x$ as not to exclude the possibility of intermediates which decompose to the previously mentioned dihydroxide and oxide. The presence of quinone may impact the direct oxidation process or the precipitation process of soluble species in subtle and nuanced ways. This is an active area of further research on the nature of these reactions.

Citations

(1) Tong, L.; Goulet, M.-A.; Tabor, D. P.; Kerr, E. F.; De Porcellinis, D.; Fell, E. M.; Aspuru-Guzik, A.; Gordon, R. G.; Aziz, M. J. Molecular Engineering of an Alkaline Naphthoquinone Flow Battery. *ACS Energy Lett.* **2019**, *4* (8), 1880–1887. https://doi.org/10.1021/acsenergylett.9b01321.

(2) Lin, K.; Chen, Q.; Gerhardt, M. R.; Tong, L.; Kim, S. B.; Eisenach, L.; Valle, A. W.; Hardee, D.; Gordon, R. G.; Aziz, M. J.; Marshak, M. P. Alkaline Quinone Flow Battery. *Science* **2015**, *349* (6255), 1529–1532. https://doi.org/10.1126/science.aab3033.

(3) Yang, Z.; Tong, L.; Tabor, D. P.; Beh, E. S.; Goulet, M.-A.; De Porcellinis, D.; Aspuru-Guzik, A.; Gordon, R. G.; Aziz, M. J. Alkaline Benzoquinone Aqueous Flow Battery for Large-Scale Storage of Electrical Energy. *Adv. Energy Mater.* **2018**, *8* (8), 1702056. https://doi.org/10.1002/aenm.201702056.

(4) Hu, P.; Lan, H.; Wang, X.; Yang, Y.; Liu, X.; Wang, H.; Guo, L. Renewable-Lawsone-Based Sustainable and High-Voltage Aqueous Flow Battery. *Energy Storage Materials* **2019**, *19*, 62–68. https://doi.org/10.1016/j.ensm.2018.10.017.

(5) Bockelmann, M.; Becker, M.; Reining, L.; Kunz, U.; Turek, T. Passivation of Zinc Anodes in Alkaline Electrolyte: Part II. Influence of Operation Parameters. *J. Electrochem. Soc.* **2019**, *166* (6), A1132–A1139. https://doi.org/10.1149/2.0791906jes.

(6) Bockelmann, M.; Becker, M.; Reining, L.; Kunz, U.; Turek, T. Passivation of Zinc Anodes in Alkaline Electrolyte: Part I. Determination of the Starting Point of Passive Film Formation. *J. Electrochem. Soc.* **2018**, *165* (13), A3048–A3055. https://doi.org/10.1149/2.0331813jes.

(7) Shin, J.; Lee, J.; Park, Y.; Choi, J. W. Aqueous Zinc Ion Batteries: Focus on Zinc Metal Anodes. *Chem. Sci.* **2020**, *11* (8), 2028–2044. https://doi.org/10.1039/D0SC00022A.

(8) Cachet, C.; Ströder, U.; Wiart, R. The Kinetics of Zinc Electrode in Alkaline Zincate Electrolytes. *Electrochimica Acta* **1982**, *27* (7), 903–908. https://doi.org/10.1016/0013-4686(82)80214-4.

(9) Debiemme-Chouvy, C.; Vedel, J. Supersaturated Zincate Solutions: A Study of the Decomposition Kinetics. *J. Electrochem. Soc.* **1991**, *138* (9), 2538–2542. https://doi.org/10.1149/1.2086013.

(10) Fenton, A. M.; Ashraf Gandomi, Y.; Mallia, C. T.; Neyhouse, B. J.; Kpeglo, M. A.; Exson, W. E.; Wan, C. T.-C.; Brushett, F. R. Toward a Mechanically Rechargeable Solid Fuel Flow Battery Based on Earth-Abundant Materials. *ACS Omega* **2022**, acsomega.2c05798. https://doi.org/10.1021/acsomega.2c05798.